Optics Letters

Heterodyne locking of a fully integrated optical phase-locked loop with on-chip modulators

Shamsul Arafin,[1,*] Arda Simsek,[1] Mingzhi Lu,[1,2] Mark J. Rodwell,[1] and Larry A. Coldren[1,3]

[1]Department of Electrical and Computer Engineering, University of California, Santa Barbara, California 93106, USA
[2]Currently at Infinera Corp., Sunnyvale, California 94089, USA
[3]e-mail: coldren@ece.ucsb.edu
*Corresponding author: sarafin@ucsb.edu

Received 7 July 2017; revised 24 August 2017; accepted 28 August 2017; posted 29 August 2017 (Doc. ID 301996); published 19 September 2017

We design and experimentally demonstrate a highly integrated heterodyne optical phase-locked loop (OPLL) consisting of an InP-based coherent photonic receiver, high-speed feedback electronics, and an RF synthesizer. Such coherent photonic integrated circuits contain two widely tunable lasers, semiconductor optical amplifiers, phase modulators, and a pair of balanced photodetectors. Offset phase-locking of the two lasers is achieved by applying an RF signal to an on-chip optical phase modulator following one of the lasers and locking the other one to a resulting optical sideband. Offset locking frequency range >16 GHz is achieved for such a highly sensitive OPLL system which can employ up to the third-order-harmonic optical sidebands for locking. Furthermore, the rms phase error between the two lasers is measured to be 8°.

OCIS codes: (250.5300) Photonic integrated circuits; (060.5625) Radio frequency photonics; (060.2840) Heterodyne; (140.0140) Lasers and laser optics; (140.3600) Lasers, tunable; (140.3945) Microcavities.

https://doi.org/10.1364/OL.42.003745

There has been a great deal of interest in millimeter/micro/terahertz-wave photonic link technology to enable a number of applications including broadband wireless communication [1] and optically fed phased-array antenna beamformers [2]. As a counterpart of noncoherent direct detection in these fiber-optic links [3], coherent remote heterodyne detection (RHD) technique offers a number of advantages, such as higher link gain and carrier to noise ratio, as well as lower sensitivity to chromatic dispersion [4]. Most importantly, one of the major building blocks in such RHD-based photonic links is the highly integrated and low-power photonic transmitter at the base station [5]. According to the RHD principle, two phase-correlated laser signals with a certain frequency offset are generated by a dual-frequency laser transmitter. Both laser signals are transmitted through the fiber link, and finally, they are mixed in a photodetector at the receiver end.

A heterodyne optical phase-locked loop (OPLL) [6] is one of the most attractive and effective techniques for achieving offset phase-locking between these two lasers of the transmitter. This suggests that a successful realization of the highly integrated OPLL is a prime requirement for developing an efficient photonic transmitter. Highly integrated heterodyne OPLLs, consisting of coherent photonic integrated receiver circuits with two widely tunable lasers, optical couplers, and a pair of balanced photodetectors—all monolithically integrated together with short delay, high-speed feedback electronics, and a tunable RF synthesizer—have been explored previously [7].

There are two techniques that could be adopted for such heterodyne locking [8]. As a first technique, the RF signal can be applied to an electronic mixer following optical detection in the feedback electronics and the RF difference frequency used for offset locking. Another technique is to apply the RF to an on-chip optical modulator monolithically integrated on the photonic receiver following one of the tunable lasers and to achieve the offset locking using an optical sideband.

There are a number of reports [6,9] that employ the former technique for demonstrating the offset locking, paving for the way to energy-efficient photonic transmitter. Due to the electronic mixer used in the first technique, the OPLL system, however, requires roughly ∼0.5 W more electrical power and extra space compared to a system based on the latter technique. In contrast, the small-area on-chip optical phase modulator operated in reverse bias requires considerably less power. Ristic *et al.* have already employed the second technique as a proof of principle demonstration of locking two sampled-grating distributed Bragg reflector (SG-DBR) lasers in InP-based photonic integrated circuits [10]. However, the OPLL system presented there suffered from small loop bandwidth, a narrow offset-locking range of 5 GHz, and slow feedback electronics with a single-ended signal coming from a photodetector.

In this Letter, we report the second technique using refined InP-based photonic integrated circuits by properly positioning the on-chip modulators for applying the RF. Agile and highly sensitive feedback electronics with a unity-gain open-loop bandwidth of 500 MHz was used [11], which utilize two photodetectors as a balanced pair. Offset locking frequency range on the order of >16 GHz is achieved in the system which can employ up to the third-order-harmonic optical sidebands for locking. A reduced phase noise of the OPLL is also obtained.

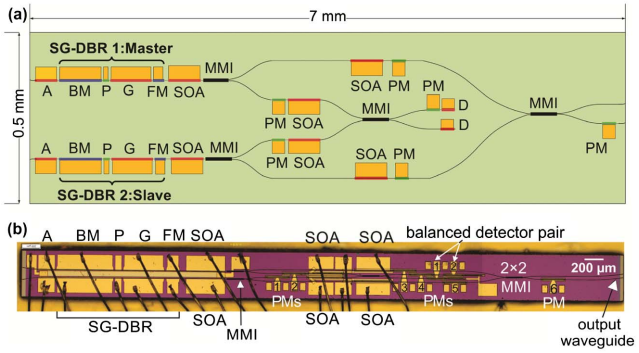

Fig. 1. Functional schematic of the coherent photonic integrated receiver circuit composed of two SG-DBR lasers, MMI couplers/splitters, SOAs, phase modulators, and a balanced photodetector pair, and (b) microscope image of the fully processed PIC mounted on a separate AlN carrier and wirebonded. (A, absorber; BM, back mirror; D, photodetector; FM, front mirror; G, gain; MMI, multimode interference; P, phase tuner; PM, phase modulators; SOA, semiconductor optical amplifier.)

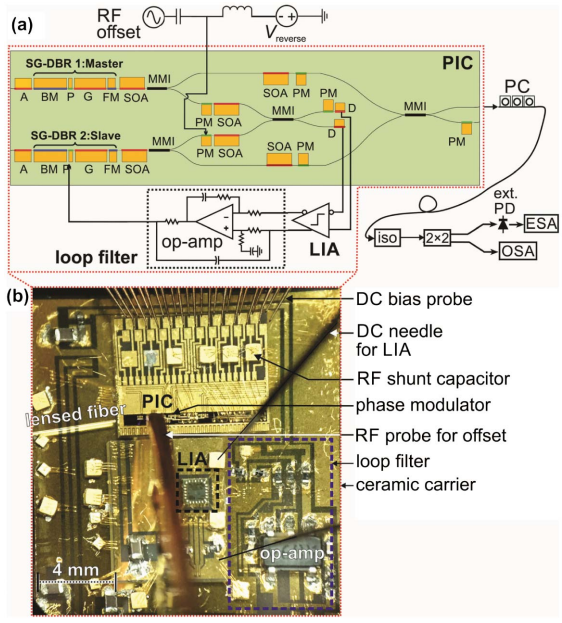

Fig. 2. (a) Test setup of the heterodyne OPLL system for confirming the phase-locking between two SG-DBR lasers. (ESA, electrical spectrum analyzer; OSA, optical spectrum analyzer; PC, polarization controller; iso, isolator; ext. PD, external photodetector; LIA, limiting amplifier; PIC, photonic integrated circuit.) (b) Optical microscope image of the OPLL system including PIC, limiting amplifier (LIA), and loop filter on a separate AlN carrier.

Figure 1(a) shows a schematic of the coherent optical receiver photonic integrated circuit (PIC) used for OPLL. It includes two widely tunable SG-DBR lasers that are to be offset locked, multimode interference (MMI) couplers, semiconductor optical amplifiers (SOAs), photodetectors, and six optical modulators. Given the wide tuning range, exceeding 40 nm in both on-chip lasers, laser outputs with frequency offsets from DC to 5 THz are possible. Among the modulators in the chip, two are for offset locking, one is for adding phase adjustments in the feedback loop, and the remaining three are for possible imposition of data on one of the two carriers that exit the chip on the right. The chip size is 7 mm × 0.5 mm.

As can be seen, light from each laser is first equally divided into two portions using 1 × 2 MMIs. One half from each laser is guided into a central 2 × 2 MMI, which is a part of the feedback loop. Each input arm of the 2 × 2 MMI contains a phase modulator that is used for applying the RF to generate optical sidebands. After combining these two lasers in the MMI coupler, light signals are detected in a pair of photodetectors (D) with a balanced receiver configuration. The other half from each laser is directed through a power boosting SOA and an optional RF signal encoding phase modulator into a 2 × 2 MMI at the far right side of the OPLL-PIC, where there are also outputs to fibers. In these experiments, these outputs are useful for monitoring the interference resulting from the beating of the two SG-DBR lasers. In practical use, these would be the outputs that would be used for RF signal remoting.

An optical microscope photo of the fully processed PIC on an InGaAsP/InP material platform is shown in Fig. 1(b). The process used to fabricate the devices is quantum-well intermixing (QWI) that creates self-aligned passive regions by intermixing the quantum-wells with their barriers and surrounding waveguide material by a patterned diffusion of implanted phosphorus ions after a first growth. Details of the processing steps for the well-established QWI-based material structure can be found elsewhere [12].

In these heterodyne OPLL experiments, one of the integrated SG-DBR lasers was used as a master, with the other as a slave to be offset phase-locked to the former. Prior to combining the outputs of these two lasers using the central 2 × 2 optical coupler, the output of the slave SG-DBR laser was intensity-modulated for offset locking using an RF offset frequency applied to its integrated on-chip modulator to create sidebands. The on-chip photodetectors generated a current response proportional to the difference frequency between the master laser and the selected sideband to which the slave laser was open-loop tuned. This current was amplified and filtered through the feedback electronics and fed back to the phase tuning section (P) of the slave laser, as schematically illustrated in Fig. 2(a). With sufficient gain in the limiting amplifier and proper integration in the loop filter, the difference frequency was driven to zero, and the phase difference between the master and slave laser fields was minimized.

Figure 2(b) shows an optical image of the assembled heterodyne OPLL system, including the PIC and the feedback electronic circuits. The electronic circuits were built by integrating a SiGe-based limiting amplifier (LIA) manufactured by ADSANTEC [13] and discrete loop filter components. These three parts were tightly integrated on a patterned aluminum-nitride (AlN) carrier by wirebonding. A DC-coupled system was prepared, since the photodetectors require reverse biasing by 2 V, which was provided from the electronic circuits. In fact, due to current mode logic (CML)-type inputs of LIA, together with the 50 Ω loads and off-chip level-shifting diodes, the LIA develops −2 V input voltage through self-biasing. In other words, the LIA directly interfaces to the PIC by reverse biasing the photodetectors by 2 V.

To summarize, the random phase variation between the two lasers translates into intensity-modulated error signals at the outputs of the 2 × 2 MMI in the PIC and finally into current

error signals at the output of the photodetectors. The error signals generated by these reverse biased photodetectors were amplified by the LIA and filtered by the loop filter. Finally, the filtered output is converted into current signals needed to control the injection of carriers into the forward-biased phase section of the slave SG-DBR laser.

To demonstrate offset locking of the slave laser to the master laser, the inner optical modulator after the 1 × 2 MMI following the slave laser was reverse biased using a bias tee. Based on the Franz–Keldysh effect through reverse bias modulation, this electro-absorption modulator generates multiple optical sidebands after applying the RF signal into it. The amount of reverse bias and magnitude of the RF determines what intensity modulation is obtained versus phase modulation. Mixing the slave laser and its associated sidebands with the master laser occurs in the photodetectors, which generate corresponding current error signals to the feedback electronics. Since the loop bandwidth of the OPLL is ∼500 MHz, only the nearest sideband(s) is amplified and fed to the phase section of the slave laser as an error signal. When the frequency separation between the two SG-DBR lasers equals the modulation frequency, the detected photocurrent will contain a phase-dependent DC component, and sideband locking of the slave laser to the master becomes possible. It should be noted that the power in the sidebands is smaller in comparison to the power at the center frequencies of the slave laser.

The combined beat signal of the slave and master lasers was coupled out from the output waveguide of the PIC using a lensed fiber for monitoring purposes. An optical isolator was used at the combined output to reduce back reflections. To measure the OPLL tone, the combined optical output passes through an off-chip 2 × 2 coupler. One output was detected via an external high-speed photodetector and measured on the electrical spectrum analyzer (ESA). The other output of this coupler was connected to the optical spectrum analyzer (OSA) to measure the optical spectra of the lasers.

Prior to performing the phase-locking between these lasers, it is important to know the optimum bias point of the on-chip modulator in order to obtain maximum modulation efficiency. Figure 3(a) shows the slave SG-DBR laser output power versus reverse bias voltage applied to the on-chip modulators located at the inner output part of the 1 × 2 MMI followed by the slave laser. Based on the characteristics shown here, approximately −3.5 V is found to be the optimum bias point of significant absorption at which the modulator was driven with strong RF signal to obtain strong sidebands beside the optical carrier and a reasonably good extinction ratio. In this case, both intensity (I) and phase modulation (PM) result. However, intensity modulation (IM) generates better sidebands than PM, considering that the on-chip modulator is driven by a strong RF tone that cannot be done without the large reverse bias. Hence, this of necessity puts our modulator in the IM regime.

Figure 3(b) shows the optical spectra of the same laser modulated at two different modulation frequencies, when the RF power of the modulation signal is kept at 17 dBm. At a modulation frequency of 10 GHz, a number of sidebands are generated with intensity comparable to that of the optical carrier. The ratio of 5 dB for the optical carrier to the first-order sideband is enough for our offset locking experiments. On the other hand, when the laser is modulated at 20 GHz, a fewer number of sidebands with reduced intensity can be observed, that is, the ratio of −8.5 dB of the first-order sideband with respect to the optical carrier is obtained. Please note that a customized GSG RF probe with a 50 Ω terminating resistor and a copper heat sink was used to launch the high-power RF signal into the reverse-biased modulator.

Figure 4(a) shows the optical spectrum when the two on-chip lasers are offset locked at ∼3.1 GHz, as determined by the RF frequency synthesizer. The OSA spectral separation between the lasers is ∼0.03 nm, which corresponds to ∼3.1 GHz. The beating tone of the locked lasers is shown in Fig. 4(b) both before and after the locking circuit is activated. The beat note has a linewidth on the order of MHz before the phase-locking. After offset phase-locking, the differential linewidth is reduced significantly, indicating strong phase-correlation between the two lasers.

Figure 5 shows a series of electrical spectra for the different offset locking conditions up to the fundamental RF frequency of 16.3 GHz. By changing the RF reference frequency to the on-chip optical modulator, these heterodyne locking conditions were obtained. The higher the offset locking range, the easier it becomes for the OPLL to track the reference signal over a broad range of frequencies. The offset locking range, pull-in range, and hold-in range of our heterodyne OPLL are measured to be ∼16 GHz, 1.2 GHz, and 1.4 GHz, respectively.

With deep phase modulation of the integrated modulator, it is possible to generate a number of side bands, and such modulators can be made with bandwidths up to ∼100 GHz [14,15], so it is anticipated that such offset locking might be possible up to the THz range without having to generate RF higher than 100 GHz. Using our heterodyne OPLL system, offset phase-locking of the lasers up to the third-order harmonic optical sidebands is obtained, as shown in Fig. 6.

The locked beat note at 2.3 GHz produced between the on-chip lasers was connected to the ESA, and the residual phase

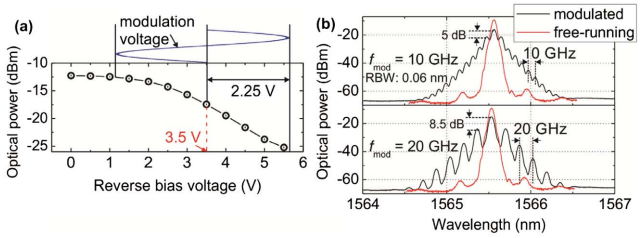

Fig. 3. Optical output power of the slave laser against reverse bias voltage applied into electro-absorption phase modulators in the PIC, and (b) optical spectra of the same laser at two different modulation frequencies applied into modulator biased at a voltage of −3.5 V.

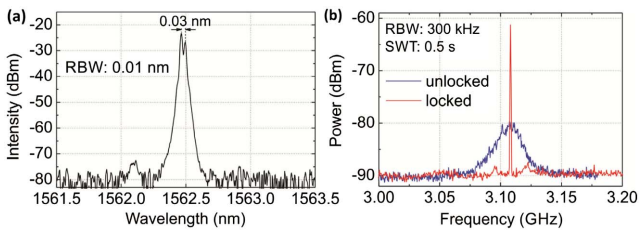

Fig. 4. (a) Optical spectrum when the two on-chip lasers that are offset locked to each other, and (b) RF spectrum of the locked beatnote between these lasers at 3.1 GHz. RBW, resolution bandwidth; SWT, sweeping time.

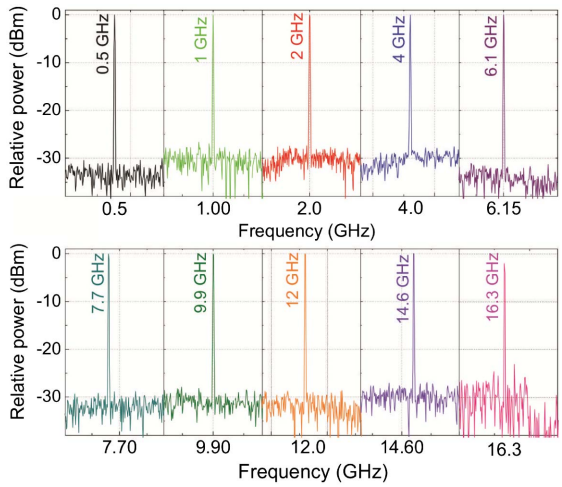

Fig. 5. Offset locking demonstrated at different offset frequencies.

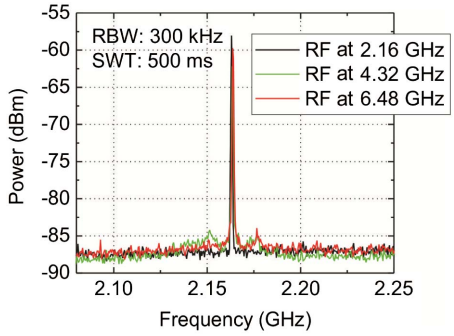

Fig. 6. Offset locking demonstrated at a fundamental RF offset frequency and up to the third harmonics.

noise spectral density (PNSD) was measured from 10 Hz to 1 GHz, as shown in Fig. 7. With a balanced photodetector pair on the chip, as well as their utilization through differential limiting amplifier based electronics, reduced noise in the feedback loop was observed. This is evidenced by the phase noise variance from 10 Hz to 1 GHz, which is calculated to be 0.02 rad^2, corresponding to 8° standard deviation from the locking point. The OPLL phase noise at low frequencies exhibits more noise compared to the RF source. This low frequency noise component is believed to be introduced by the measurement setup, such as fiber vibration and AM-to-PM conversion in the ESA, rather than the OPLL system itself [12]. The phase noise at high frequencies might be caused by the relative intensity noise of the laser.

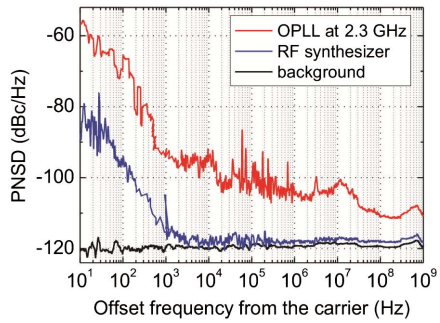

Fig. 7. Single-sideband residual phase noise of the heterodyne OPLL. Phase noise of the RF synthesizer and background are also shown here for comparison.

In this work, we have successfully demonstrated a highly integrated OPLL by employing PICs with all optical master and slave SG-DBR lasers, high-speed modulators, high-speed photo detectors, MMI couplers, and interconnecting optical waveguides. An experiment to demonstrate offset (up to ~16 GHz) locking of the master and slave SG-DBR lasers is performed. Future works involve the use of high bandwidth on-chip phase modulators and high-gain limiting amplifier in order to achieve offset locking with higher-order-harmonic optical sidebands. Hence, our OPLL is expected to generate phase stable optical beat at very high frequencies.

Funding. GOALI project, National Science Foundation (NSF) (1402935).

REFERENCES

1. T. Nagatsuma, S. Horiguchi, Y. Minamikata, Y. Yoshimizu, S. Hisatake, S. Kuwano, N. Yoshimoto, J. Terada, and H. Takahashi, Opt. Express **21**, 23736 (2013).
2. L. N. Langley, M. D. Elkin, C. Edge, M. J. Wale, U. Gliese, X. Huang, and A. J. Seeds, IEEE Trans. Microwave Theory Tech. **47**, 1257 (1999).
3. Z. Qiang, X. Changsong, N. Stojanovic, G. Goeger, S. Chun, F. Yuanyuan, Z. Enbo, L. Gordon Ning, and X. Xiaogeng, in *Opto-Electronics and Communications Conference* (IEEE, 2015), paper JTuA.41.
4. U. Gliese, T. N. Nielsen, S. Nørskov, and K. E. Stubkjær, IEEE Trans. Microwave Theory Tech. **46**, 458 (1998).
5. Y. Shoji, IEICE Trans. Electron. **E88-C**, 1465 (2005).
6. S. Arafin, A. Simsek, S. K. Kim, S. Dwivedi, W. Liang, D. Eliyahu, J. Klamkin, A. Matsko, L. Johansson, L. Maleki, M. Rodwell, and L. A. Coldren, Opt. Express **25**, 681 (2017).
7. K. Balakier, L. Ponnampalam, M. J. Fice, C. C. Renaud, and A. J. Seeds, IEEE J. Sel. Top. Quantum Electron. **24**, 1 (2017).
8. L. A. Coldren, M. Lu, J. Parker, L. Johansson, S. Arafin, D. Dadic, and M. J. Rodwell, *Advanced Photonics Congress* (Optical Society of America, 2016), paper JM1A.2.
9. S. Arafin, A. Simsek, S. K. Kim, W. Liang, D. Eliyahu, G. Morrison, M. Mashanovitch, A. Matsko, L. Johansson, L. Maleki, M. J. Rodwell, and L. A. Coldren, IEEE Photon. J. **9**, 1 (2017).
10. S. Ristic, A. Bhardwaj, M. J. Rodwell, L. A. Coldren, and L. A. Johansson, J. Lightwave Technol. **28**, 526 (2010).
11. A. Simsek, S. Arafin, S.-K. Kim, G. Morrison, L. A. Johansson, M. Mashanovitch, L. A. Coldren, and M. J. Rodwell, *Optical Fiber Communication Conference* (Optical Society of America, 2017), paper W4G.3.
12. M. Lu, "Electrical and computer engineering," Ph.D. dissertation (University of California Santa Barbara, 2013).
13. http://www.adsantec.com/344-asnt5020-bd.html.
14. Y. Ogiso, J. Ozaki, Y. Ueda, N. Kashio, N. Kikuchi, E. Yamada, H. Tanobe, S. Kanazawa, H. Yamazaki, Y. Ohiso, T. Fujii, and M. Kohtoku, J. Lightwave Technol. **35**, 1450 (2017).
15. P. Evans, M. Fisher, R. Malendevich, A. James, G. Goldfarb, T. Vallaitis, M. Kato, P. Samra, S. Corzine, E. Strzelecka, P. Studenkov, R. Salvatore, F. Sedgwick, M. Kuntz, V. Lal, D. Lambert, A. Dentai, D. Pavinski, J. Zhang, J. Cornelius, T. Tsai, B. Behnia, J. Bostak, V. Dominic, A. Nilsson, B. Taylor, J. Rahn, S. Sanders, H. Sun, K.-T. Wu, J. Pleumeekers, R. Muthiah, M. Missey, R. Schneider, J. Stewart, M. Reffle, T. Butrie, R. Nagarajan, M. Ziari, F. Kish, and D. Welch, Opt. Express **19**, B154 (2011).